Long Time Evolution of Structural Hierarchy in Uniaxially Stretched and Retracted Cross-Linked Natural Rubber

D. Valladares, B. Yalcin, and M. Cakmak*

Polymer Engineering Institute, University of Akron, Akron, Ohio 44325-0301

Received February 27, 2005; Revised Manuscript Received August 11, 2005

ABSTRACT: The long time evolution of structural hierarchy in cross-linked natural rubber, i.e., *cis*-polyisoprene, was investigated in uniaxially stretched and partially retracted state using real time birefringence, optical microscopy, and wide angle X-ray scattering techniques. During the deformation, the needlelike domains that contain highly oriented crystals develop in the stretching direction. The constrained holding of these samples up to 14 days results in the development of additional crystals adjacent to original needlelike domains exhibiting lower orientation. Further holding up to 47 days results in lateral overgrowths of lamellar crystals emanating from these oriented crystals. Growth branching was found to be increasingly suppressed with the long-term crystallization that lead to the formation of two-dimensional crystals that grew the longest. Slight retraction after stretching results in a higher crystalline orientation with lower crystallinity due to retraction-induced melting of crystalline regions with lower orientation. The population of lateral lamellar overgrowths on oriented crystals was found to be larger in these stretched and retracted samples than the samples subjected to stretching only. Temperature dependent WAXS analysis of these crystallites in stretched and stretched−retracted samples indicates that the crystals with differing perfection and tilt angle with respect to the stretching direction melt earlier than their more perfectly aligned counterparts.

1. Introduction

The crystallization of natural rubber can take place through thermal and/or and strain-induced mechanisms. The fundamental understanding of both mechanisms is of great importance for the rubber industry as they influence the behavior of the material in processing and actual use conditions. The thermally induced crystallization is significant in rubber applications that are subjected to low temperatures as well as long duration holding at room temperature. The occurrence of crystallization is not desirable in most applications as it inhibits the characteristic elastic response of this material. On the other hand, the ability of natural rubber to crystallize under deformation even at temperatures higher than its apparent melting point is highly desirable for applications that require momentary property changes to prevent the crack growth leading to the arrest of failure.

Crystallization of natural rubber depends on various factors including temperature and time of crystallization,[1] pressure,[2,3] deformation,[4,5] cis−trans configuration,[6] side groups,[7] cross-link density,[8] impurities, and nonrubber components such as proteins and phospholipids.[9,10] Nonrubber components were recently shown to be an important factor in the formation of gel points that provide heterogeneous nucleation sites for rubber. The gel points (branch points) are associated with the interactions of the nonrubber constituents, i.e., proteins and fatty acids, with the hydrocarbon chains of the rubber over time.[11] Gel formation during storage contributes to the hardening and inelasticity of the rubber.[12]

In the absence of deformation, natural rubber thermally crystallizes into spherulitic structure at temperatures between +20 and −50 °C with the maximum crystallization rate located at about −26 °C.[1 4] Several researchers determined the equilibrium melting temperature ($T_m°$)[13−17] that is defined as the thermodynamic melting temperature of a perfect crystal. The calculated values of $T_m°$ for natural rubber coagulated from the latex and purified rubber is about 28 °C.[17] Higher values were also reported for $T_m°$, 35.5 °C, of natural rubber at atmospheric pressure.[14,15]

Strain-induced crystallization of rubber is an important and a well researched area with publications dating back to 1940s. Crystalline morphology of natural rubber under strain was first discussed by Andrews[5] following the work of Scott who recognized that strain-induced morphology in polymers is in general anisotropic and consists of fibrillar structures in the direction of strain.[18] Andrews's discussions were based on the transmission electron microscopy (TEM) observations of the unvulcanized natural rubber thin films isothermally crystallized at temperatures between −20 and −30 °C.[5] He showed that the crystalline phase of natural rubber takes on different morphologies depending on the level of strain applied prior to isothermal crystallization. At low to moderate prestrain levels (100−200%), filaments grow perpendicular to the stretching direction along the *a*-crystallographic axis (α-filaments) and stack on top of each other forming row structures in the stretching direction. At high prestrains (500−800%), α-filaments disappear and the newly forming *γ*-filaments preferentially orient with their *c*-crystallographic axis parallel to the stretching direction. Andrews suggested that *γ*-filaments were actually the nuclei of the α-filaments formed spontaneously at high strains. The increase in the nucleation density at high strains (500−800%) suppressed the lateral growth leading to the appearance of filaments oriented in the stretching direction. The nature and the mechanism of the *γ*-filament growth as explained by Andrews required fairly short lamella to grow laterally while stacking on top of each other in the

* Corresponding author. E-mail: Cakmak@uakron.edu. Telephone: 330-972-6928.

10.1021/ma050413q CCC: $30.25
Published on Web 10/07/2005

stretching direction as soon as the natural rubber was prestretched. With further studies[19] including electron diffraction, it was shown that if there was no crystalline diffraction from pre-strained natural rubber samples before the isothermal crystallization, no edge on lamella (α-filaments) was present after isothermal crystallization. This implied that the γ-filaments that form immediately by prestretching correspond to "shish" crystals and act as templates on which the lamellae nucleate and grow laterally during isothermal crystallization stage. In the lightly stretched samples, the γ-filaments are present but are too slender to be seen by TEM. In moderately prestretched rubber, the lateral growth of the lamella on the shish crystals is greater since the population of these shish crystals is not large enough to cause impediment to the lateral growth. In summary, γ filaments—shish crystals—form immediately by prestretching and the α-filaments grow on the shish crystals perpendicular to the stretching direction during isothermal crystallization. A less stable lamellar crystal, namely β-lamellae, that possess the same crystal structure as that of α lamellae but a different crystallographic growth face (110) was subsequently identified by Edwards.[20] Both α and β lamellae can be present in the same *cis*-polyisoprene spherulite as well as on the same shish structure as lateral growths.[21] The presence of β-lamellae can be influenced by the chemical microstructure at low levels[22] and at high pressures β population was found to be suppressed due to substantial increases in the growth rate of α form.[23]

Strain-induced crystallization of natural rubber, pioneered by Andrews, Edwards, and Phillips, is still the subject of interest for many researchers after almost 60 years. In most of these studies, the rubber was unvulcanized and free of impurities. The crystallization and melting processes in vulcanized stretched natural rubber was recently reported in detail.[8] The authors showed that cross-links in the natural rubber impede the rearrangement of the crystallites and limit the final extent of crystallinity and crystallite size.[8]

Recent in-situ WAXD synchrotron studies on cross-liked rubbers[24,25] showed the existence of a significant amount of isotropic (unoriented) amorphous phase (50−75%) even at very high strains. The oriented phase is composed of the strain-induced crystalline regions (20%) and amorphous short chains (5−25%) that act as tie between the crystallites.

In this study, we investigate the time evolution of structure in stretched cross-linked samples held in the constrained state for *very long* periods of time at ambient temperature (20 °C). We also investigate the effect of partial retraction on the long-term structural evolution of crystallites on strained samples. To elucidate the thermal behavior of the developed structure we also performed temperature-dependent WAXS analyses.

2. Experimental Section

2.1. Material. Standard Malaysian Rubber (SMR L) low impurity grade natural rubber was used in this study. SMR L contains typically around 93% of the polyisoprene hydrocarbon. The main nonrubbers are about 0.5% of nitrogen compounds, 3% protein, and about 3% acetone-extractable material. These nonrubber constituents were not removed from the SMR L rubber.

2.1.1. Compounding. The chemical ingredients for compounding are listed in Table 1. Compounding was carried out in a Brabender internal mixer followed by a two roll mill. The Brabender mixing chamber was preheated to 70 °C. The natural rubber was first introduced into the chamber and was mixed for 3 min at 60 rpm in order to complete the mastication process. Following this step, antioxidant was added into the mixing chamber. The remaining ingredients—zinc stearate, TBBS accelerant, and finely micropowdered sulfur (rubbermaker's superfine sulfur)—were added in the order specified. In this formulation zinc stearate was used instead of a mixture of zinc oxide and stearic acid since zinc oxide greatly reduces the clarity of the final vulcanizates that was essential for birefringence experiments.

Table 1. Formulation of the Natural Rubber Samples

ingredient	recipe (parts)
SMR-L	100
antioxidant	1
zinc stearate	4.5
TBBS accelerant	1.5
sulfur	1.5

The mixtures obtained by the internal mixer were further mixed with a two-roll mill to ensure a homogeneous dispersion and distribution of all ingredients in the rubber matrix. The temperature of the rolls was set to 70 °C, and a total mixing time of about 10 min was used for all mixtures.

2.1.2. Vulcanization. The compound obtained from the two roll mill mixing step was cut into 10 × 10 cm square samples and were placed in a 1 mm thick mold frame sandwiched between two metal plates. The samples were covered with a Kapton film to prevent the adhesion of rubber to the metal plates and to obtain smooth surface finish. The rubber was compression molded for 1 h at 145 °C.

The average molecular weight between the cross-links (M_c) was determined by Young modulus measurements, which is also in good agreement with the swelling techniques. We used the semiempirical equation suggested by Mooney−Rivlin (eq 1).

$$\mathrm{M_c} = \mathrm{A}_{\varphi}\, \rho \mathrm{RT}/G_e \tag{1}$$

where $\mathrm{M_c}$ = average molecular weight between cross-links, A_{φ} = prefactor (assumed to be 1), ρ = density of the rubber, R = gas constant, T = temperature, and G_e = modulus.

Modulus, G_e, which depends on the cross-link density, is related to the stress (σ) and extension ratio (λ) through eq 2. We calculated G_e from the slope of the straight line plot, σ vs $(\lambda^2 - \lambda^{-1})$.

$$\sigma = \sigma_0 + \mathrm{G_e}\,(\lambda^2 - \lambda^{-1}) \tag{2}$$

M_c of the vulcanized rubber used in this study was 6680 g/mol. Average number of monomers between cross-links, N_c, is another frequently employed cross-link density parameter and can be found by dividing M_c by the molecular weight of the monomer ($M_w = 68$). The value of N_c in this study is 98.

2.2. Instrumentation of the Uniaxial Stretcher and Sample Stretching. The uniaxial stretching experiments were carried out using a custom built instrumented uniaxial stretching system shown in Figure 1. The system allows the real time determination of true stress, true strain, and birefringence simultaneously during deformation. Although the details of this equipment and measurements were given elsewhere,[26] below we provide a brief overview.

On-line spectral birefringence is essentially based on the method described by Posthuma de Boer et al.[27] In this method, white light is used as the light source to get the order number of retardation automatically. To determine the birefringence, the thickness must be measured at the same time and at the same location where the birefringence is measured. This is accomplished using a laser micrometer mounted at an oblique angle that measures the width of the sample continuously. We then use the uniaxial symmetry (eq 3)) to calculate the real time thickness (eq 4) with the knowledge of the initial thickness. The true stress is defined as the ratio of the tensile force to the "actual" instantaneous cross section of the sample.

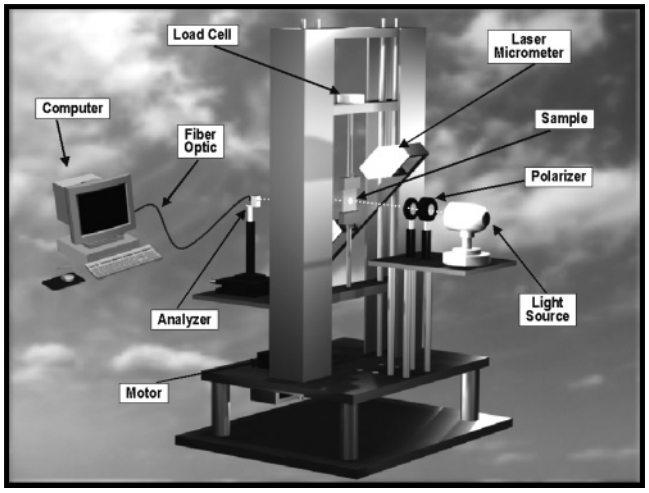

Figure 1. Spectral-birefringence stretching machine.

To get the true stress (eq 6), we directly measure tensile force by a load cell and divide it by the real time cross sectional area of the film. The real time cross sectional area of the film is the product of the width determined by the laser micrometer and the calculated thickness (eq 4). For elongation we define three parameters, i.e., stretch ratio, engineering strain and true strain. Stretch ratio is the ratio of the final length of the stretched sample to its initial length. Engineering strain is defined as the ratio of elongation (difference between the final length and the initial length) to the initial length of the sample. As for the true strain, we relate the state of elongation directly to the reduction in the local width of the sample. This is the same local region (mid region of the sample) where the retardation measurements are made. We then combine the uniaxial symmetry (eq 4) with the incompressibility assumption (eq 5) and determine the true strain (eq 7).

The incompressibility assumption is reasonable as the volume change associated with crystallization is small in natural rubber.[28] The density for fully crystalline rubber is 1.008 g/cm^3 as determined from the unit cell of Bunn.[29] The amorphous density is 0.9184 g/cm^3. For a stressed rubber, the crystallinity values can reach up to 30%.[30] The associated volume change at 30% crystallinity is about 2.6%.

$$W_t/W_o = D_t/D_o \tag{3}$$

$$D_t = \left(\frac{W_t}{W_o}\right)D_0 \tag{4}$$

$$D_o W_o L_o = D_t W_t L_t \tag{5}$$

$$\text{true strain} = \frac{\text{elongation}}{\text{initial length}} = \frac{L_t - L_o}{L_o} = \frac{\Delta L}{L_o} = \left(\frac{W_o}{W_t}\right)^2 - 1 \tag{6}$$

$$\text{true stress} = \frac{\text{force}}{\text{cross-sectional area}} = \frac{F_t}{W_t D_t} = \frac{F_t}{[(W_t^2/W_o)D_o]} \tag{7}$$

where W_t = real time width of the film, W_o = initial width of the film, D_o = initial film thickness, D_t = real time film thickness, L_o = initial length of the film, L_t = real time length of the film, and F_t = force.

Samples for stretching were prepared by cutting the compression molded sheets into dumbbell shaped samples with 8 cm × 6 cm × 1.0 ± 0.1 mm dimensions. The initial thickness of each sample and length was measured using a precision thickness gauge prior to stretching and entered in the stretching program. All the stretching experiments were performed at room temperature and at the same speed 30 mm/min. One set of samples were stretched 5.5 and 6 times (6×) their original length. Another set of samples were stretched to 6× and immediately retracted to 5.5× and 4× to investigate the effect of partial retraction on the immediate and long-term evolution of structure. Virgin samples were used for each stretching experiment. After applying these deformation prehistories, the mid portion of the stretched samples were securely clamped between the two metal rectangular frames (thickness ~4 mm) that are held together by four screws at the corners (Figure 2). With the help of serrated surfaces facing the stretched samples, these clamps prevented any possibility of slippage during long holding periods practiced in this research. The samples were kept in the darkness at room temperature.

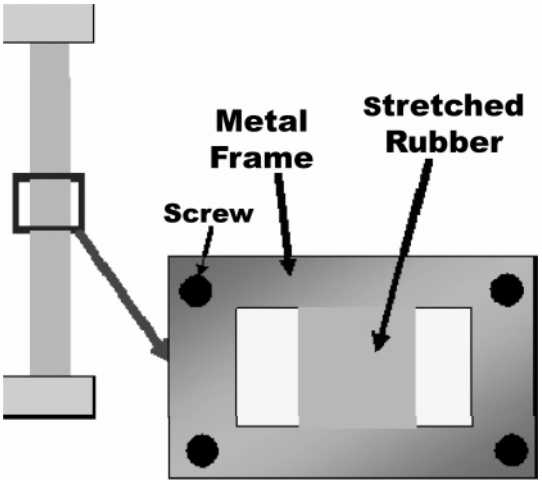

Figure 2. Rubber clamping mechanism for long-term storage in the stretched state.

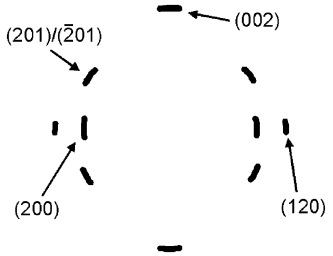

Figure 3. X-ray diffraction planes of natural rubber.

2.3. Analysis of the Crystalline Phase during Storage. Changes in the degree of crystallinity and the orientation of the crystal planes during long-term storage were studied by wide-angle X-ray scattering (WAXS). GE XRD-6 X-ray generator (40 kV and 30 mA) equipped with a SAXS/WAXS combination camera was used to obtain WAXS film patterns for samples kept in the stretched state under ambient temperature for 0, 14, 21, 29, and 47 days. Exposure time of 1.5 h was used. The most significant diffraction intensities observed for stretched natural rubber samples belong to (200), (120), (002) and (201)/(−201) crystalline diffraction planes as shown in Figure 3.

2.3.1. Crystallinity. The development of crystallinity was indirectly monitored using normalized azimuthal intensity profiles of the crystal planes on the wide-angle X-ray scattering patterns. For this purpose, the WAXS film patterns were digitized with a 12 bit linear CCD camera from Photometrix. Using exposure calibration strips, the nonlinearity in film sensitivity to the X-ray intensity was corrected. The amorphous background was then subtracted from the azimuthal intensity profiles of each of the crystalline planes (200), (120), and (201)/(−201). Integrated azimuthal intensity under the normalized peaks were then determined for a series of room temperature holding times.

2.3.2. Orientation of the Crystal Phase. Orientation of the crystal planes was determined using Wilchinsky's method.[31] We have used the monoclinic unit cell (a = 12.46 Å, b = 8.89 Å, c = 8.10 Å, and β = 92°) proposed by Bunn.[29] Azimuthal

intensity scans along the (200) and (120) planes were made in order to calculate the $\cos^2\chi_{(200)}$ and $\cos^2\chi_{(120)}$ values. Using eq 7 derived using Wilchinsky's rule,[31] the orientation factor f_c was calculated from the eq 6.

$$f_c = \frac{3\cos^2\chi_c - 1}{2} \tag{6}$$

where

$$\langle\cos^2\chi_c\rangle = 1 - 1.1317\,\langle\cos^2\chi_{(120)}\rangle - 0.8692\,\langle\cos^2\chi_{(200)}\rangle \tag{7}$$

2.3.3. Direct Observation by Optical Microscopy. A Leitz Laborlux 12 Pol optical microscope was used to observe the crystal structures grown in the stretched samples. Cross-polarized light along with a first-order red wave (λ) plate was used to determine the optical anisotropy directions in the individual crystals.

2.4. Crystal Melting Experiments. The melting temperature of the samples was obtained using three different methods:

Method 1: Hot Stage and Optical Light Intensity. This method was used for un-stretched rubber samples. A hot stage mounted on the optical microscope was set to heat the rubber samples from 20 to 50 °C at a rate of 1 °C/min. A video camera mounted on the microscope was used to take optical pictures every 30 s at the same position during the heating process under crossed polarizers. The intensity of the digital pictures obtained at each temperature was determined. The area under the intensity curve obtained at each temperature was calculated and plotted against temperature in order to determine the melting transition of the specimen.

Method 2. The stretched samples constrained in the metal frame did not fit in the hot stage device. Therefore, another method of heating, i.e., hot air blower, was employed. The temperature and heating rates are more difficult to control with the hot air blower method. For that reason, unstretched natural rubber samples were also analyzed by this method for comparison with the results from hot stage. Both results are in good agreement.

During the heating, the temperature is controlled using a thermocouple placed in contact with the bottom surface of the rubber film. The thermocouple is placed in contact with the sample approximately 500 μm away from the region of interest to ensure more realistic temperature values in the field of view. Digital pictures were taken at different temperatures. The data analysis is similar to the one used and described in the hot stage method.

Method 3: WAXS Measurements. X-ray patterns of the stretched rubber samples held between the metal frames were taken offline at a series of temperatures using a Bruker AXS X-ray machine equipped with a 2D wire detector. The exposure time was 3 min. An adjustable light source provided controlled heat allowing the control of the temperature of these constrained rubber samples. The temperature at the center of the sample was monitored using a noncontact infrared pyrometer. The disappearance of the crystalline planes was observed directly on the X-ray patterns and their intensities were recorded. Orientation factors during melting were calculated for these X-ray patterns from Wilchinsky's rule[31] using the above eqs 6 and 7.

3. Results and Discussions

The true stress-true strain behavior and the real time birefringence monitored during the stretching are shown for samples stretched to 5.5×, 6×, 6× retracted to 5.5× and 6× retracted to 4× in Figures 4 and 5, respectively. The deformation histories of the samples are quite repeatable as they superimpose during the stretching and retraction phases. The real time birefringence also follows the same trajectory during stretching and retraction.

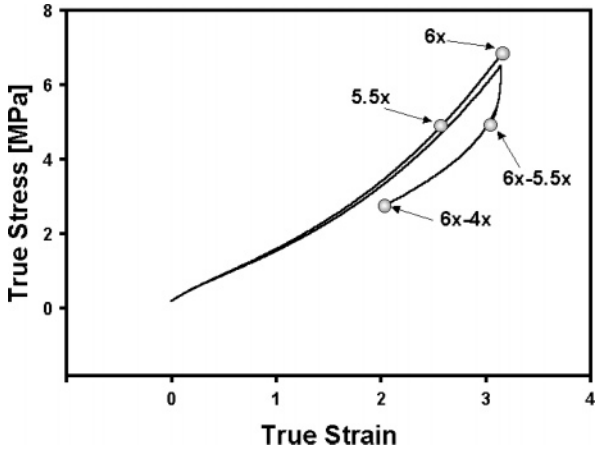

Figure 4. True stress−true strain behavior during deformation of natural rubber samples to be analyzed in time.

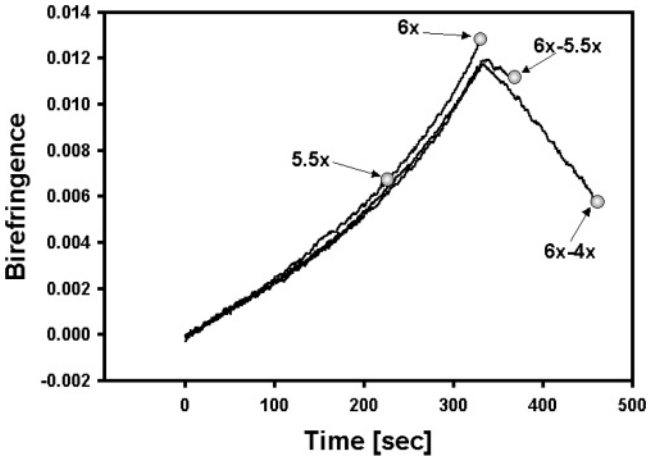

Figure 5. Real-time birefringence during deformation of natural rubber samples to be analyzed in time.

3.1 Optical Microscopy. Figure 6 shows the optical micrographs of a rubber sample stretched to 6× at room temperature. The pictures were taken immediately after the deformation process with the stretching direction oriented at 0 and 45° with respect to the polarizer. Comparison of the optical micrographs indicates the existence of high degrees of orientation anisotropy built up in the highly stretched samples. Figure 6b is considerably darker than Figure 6a as the principal axis directions of the sample optical indicatrix coincide with the polarizer and analyzer directions. The highly oriented crystalline phase contributes to this anisotropy as evidenced by the WAXS pattern. On the other hand, our analysis and those of others[24,32] indicate that the amorphous phase shows a mild anisotropy as evidenced by a near-isotropic azimuthal intensity distribution of the amorphous halo in the WAXS patterns. Only those amorphous chains that are linked through cross-links are susceptible to orientation. These chains appear to be responsible for the early development of birefringence. This is elaborated in a recent publication[24] that indicates that some of the fatty acids are integrated with the cross-linked network as they are located at the ends of some of the rubber chains[33] and become oriented from very early stages of deformation before the appearance of the crystalline peaks from the rubber phase. Vast majority of chains that are not part of the network remain unoriented. The appearance of mild orientation in the amorphous phase, thus, has two components: one

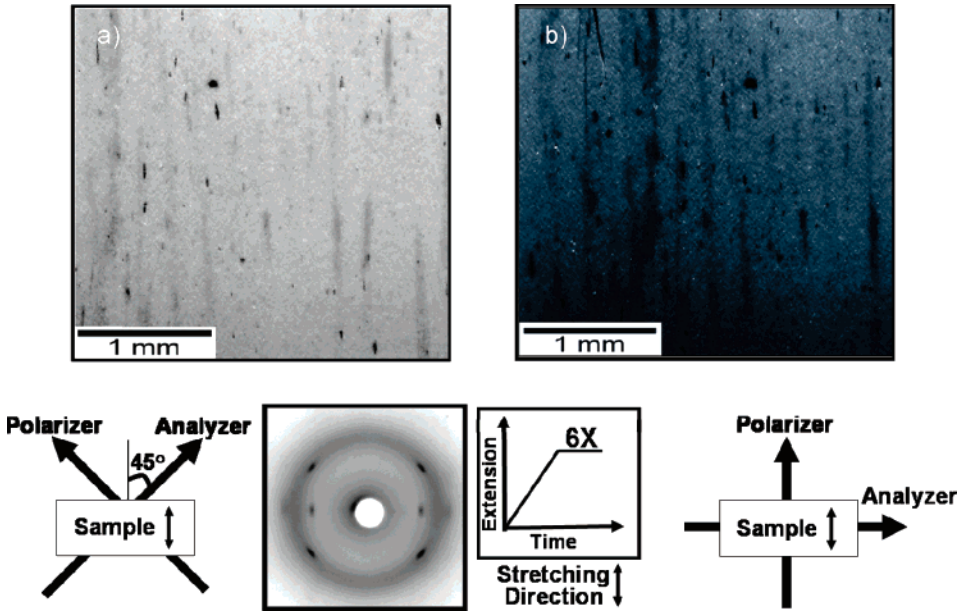

Figure 6. Optical micrographs: (A) stretching direction at 45° to the polarizer; (B) stretching direction parallel to the polarizer.

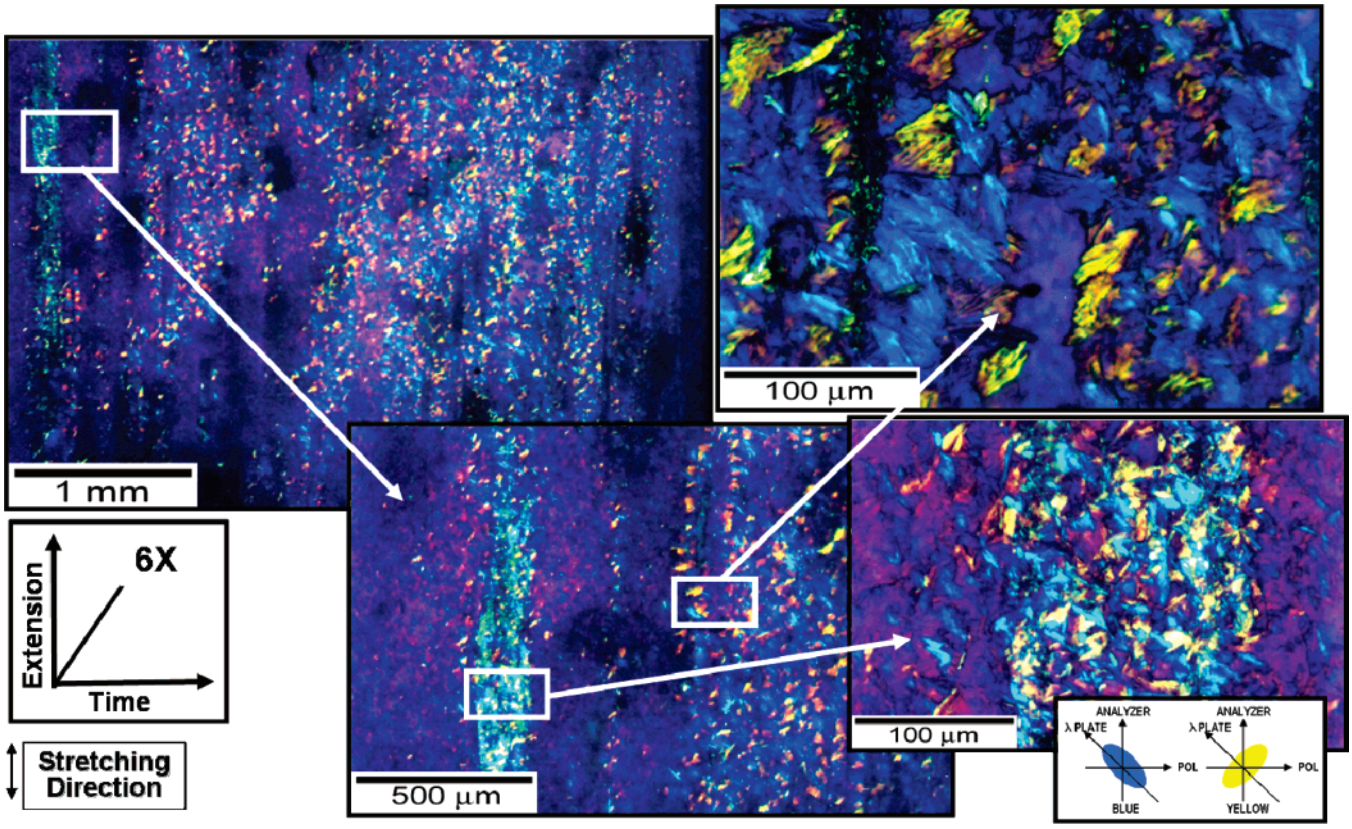

Figure 7. NR stretched to 6× and constrained for 47 days. Optical micrographs at different magnifications at location 1.

is the unoriented amorphous chains and the other is the small fraction of chains constituting the long range connected network that increasingly become oriented with deformation.

The extremely narrow azimuthal distribution of the crystallographic planes indicates that the crystalline regions are needlelike possessing very high chain axis orientations. However, these structures are not large enough to be observed by optical microscopy. The dark lines along the stretching direction in both pictures are surface irregularities; originally pores on the rubber sample that deformed along with the stretching.

After holding the sample for 47 days at room temperature (Figure 7), we observe the appearance of crystallites that were not present in the as-stretched samples. These structures are not randomly formed, but they are organized along the regions that are oriented in the stretching direction. High magnification pictures (320×) using a λ plate placed at 45° to the analyzer−polarizer (Figure 8) shows that these structures grow laterally. A striking feature of these lateral overgrowths is their thin flexible platelike shapes. Depending on the orientation of their slow axis relative to the slow axis direction of the λ plate they exhibit blue or yellow colors.

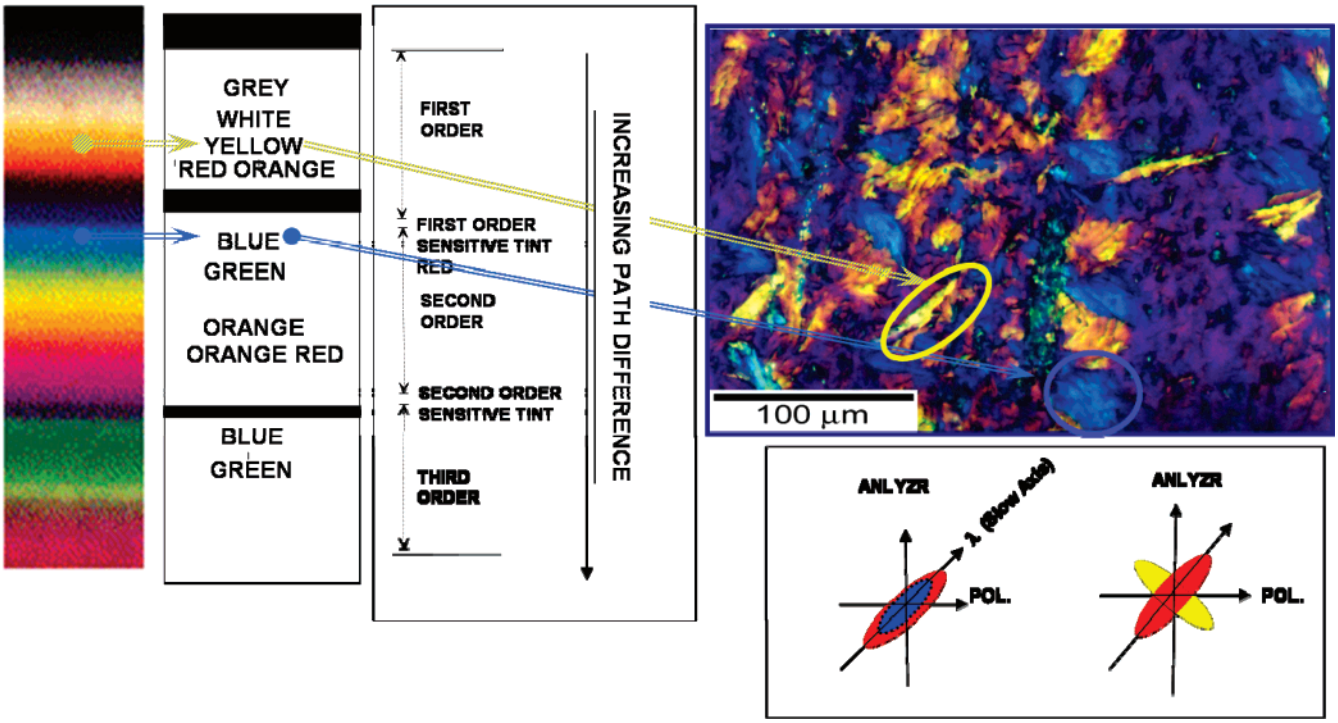

Figure 8. λ plate information on a NR stretched and constrained for 47 days optical micrograph.

Those segments that appear yellow have their slow axis (high refractive index) normal to the slow axis of the λ plate as they are in the optical subtraction orientation. Segments that appear blue have their slow axes parallel to the slow axis of the λ plate and are in addition orientation. Since the natural rubber has positive intrinsic birefringence in both the crystalline $\Delta n^\circ_c = 0.014$[34] and the amorphous $\Delta n^\circ_a = 0.02$[32] phase, the refractive index is the highest along the chain axis. The edge-on view of the 2d crystal protrusion colors indicate that the chain axes are oriented normal to the plane of these "platelike" crystals. The uniformity and large coverage area of each color region indicates structural uniformity within each "plate" (Figures 7 and 8).

As implied in these results, the highly extended chain crystals formed during stretching act as nucleating sites for these crystals to grow. The thin-platelike crystals growing laterally coats these oriented crystals leading to the formation of large shish-kebab structures. As they grow out, their growth direction deviate from radial direction and hence they demonstrate above-described colored appearance depending on the orientation of the sheet plane relative to the slow axis of the λ plate.

The lateral growth of the lamellar crystals with temperature and time on the extended shish structures in strained natural rubber is not new.[5,35] What is interesting in this report is that the lateral crystal growths in the highly stretched samples are grown to considerable size levels over time to form aggregates visible under the polarized microscope. Surprisingly, these platelike crystals show little tendency to branch at their most extended position. This can be observed in Figure 9a, where the furthest protrusions of these thin crystallites in to the noncrystalline regions are clearly shown.

It is well-known that molecular orientation of polymer chains changes the driving force and even the mechanism of crystal growth. Molecular orientation decreases the entropy which in turn increases the melting temperature of the polymers.[35] The increase in melting temperature brings the system to a supercooled state that leads to high nucleation rates of extended chain segments and their growth in the direction of stretching and hence the shish structures. Once formed, the surfaces of these shish structures act as templates on which the secondary crystallization proceeds at room temperature. Although the ability of natural rubber chains to diffuse and add onto the growing crystallites is highly suppressed due to the presence of cross-links,[8] driving force for crystallization still exists due to the increased supercooling caused by preferred orientation in the vicinity of the shish structures. We suspect that once the shish structures have formed, the preferred orientation of the polymer chains gradually decrease in the regions radially away from the shish surfaces. In other words, we do not expect the orientation to abruptly decrease beyond the boundary of the each formed shish but be an unknown decreasing function with distance from each shish. As a result, the amorphous chains near the shish regions possess higher orientation (and thus lower entropy) and higher equilibrium melting temperature (albeit less than those inside the shish regions that already caused the crystallization). This provides added driving force for the crystallization to occur once sufficient relaxation has taken place to promote crystallization[35,36] As Flory explained, once the crystallization occurs, the surrounding crystal formation brings about stress relaxation of the surrounding amorphous chains. These amorphous chains can rearrange to add on to the laterally growing crystallites over long periods of time. As the distance from each shish surface is increased, this leads to decline of the entropy advantage, and as a result, we observe rapid decrease of spatial density of kebab growths. This process takes place slowly since the probability of the natural rubber chains to diffuse is low at these temperatures. Eventually, the rate of crystallization will decrease since the degree of supercooling becomes smaller as crystallization progresses away from the oriented regions. A simple model illustrates this phenomenon in Figure 9b. Similar effects have been

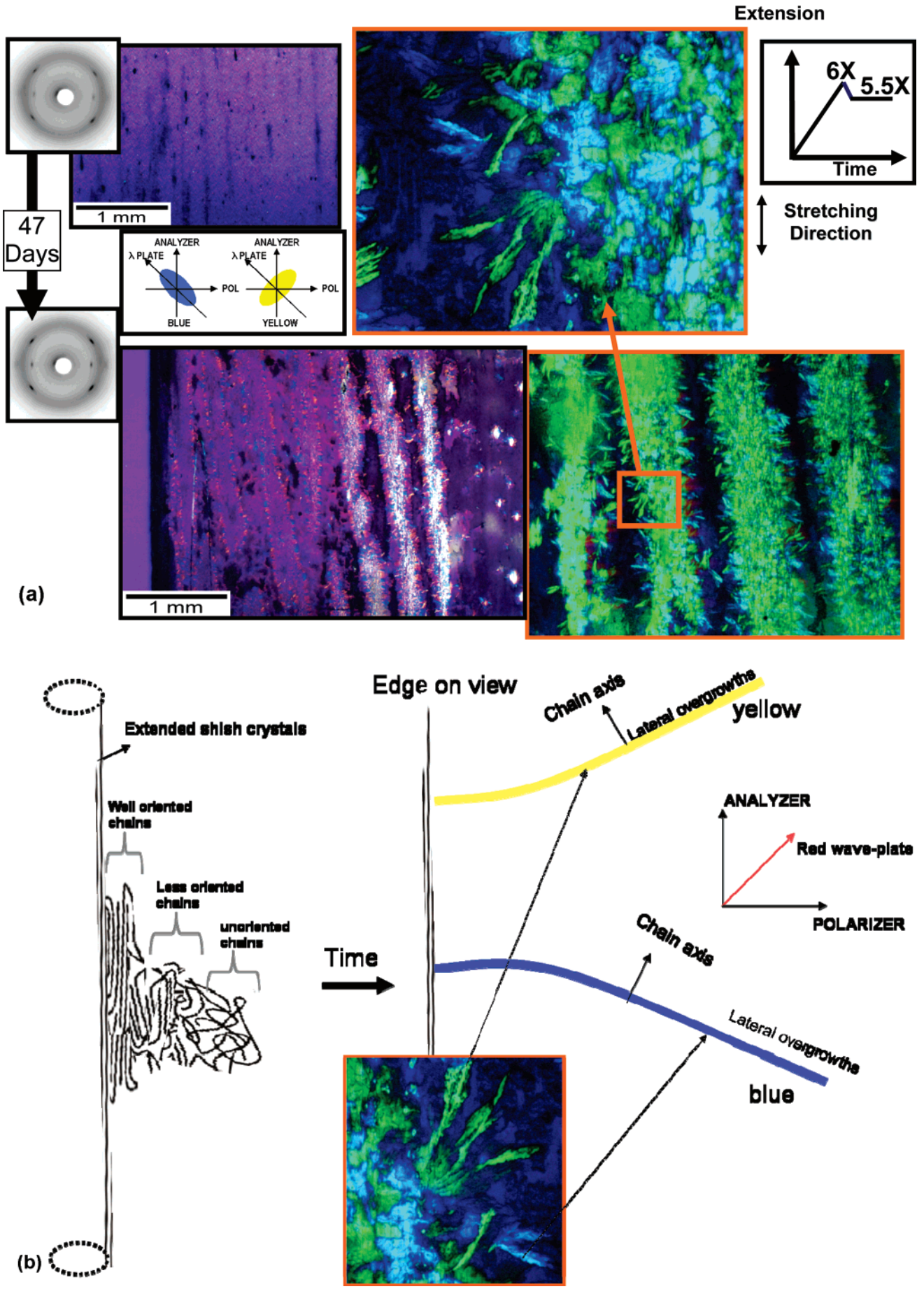

Figure 9. (a) NR stretched to 6× then retracted to 5.5× and constrained for 47 days. Optical micrographs at different magnifications at location 1. (b) Model depicting lateral overgrowth from shish crystals.

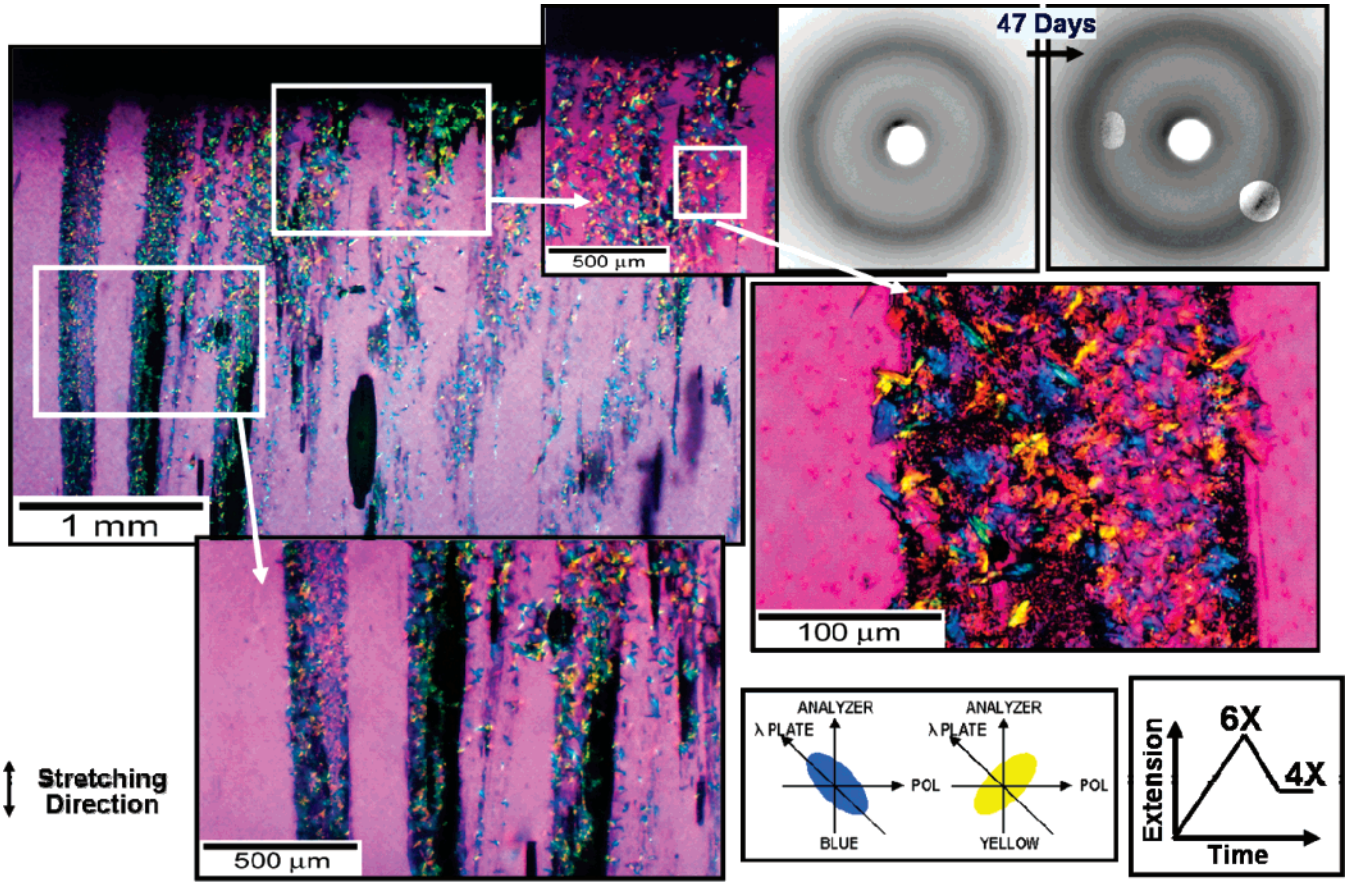

Figure 10. NR stretched to 6× and then retracted to 4× and constrained for 47 days. Optical micrographs were taken at different magnifications at location 1.

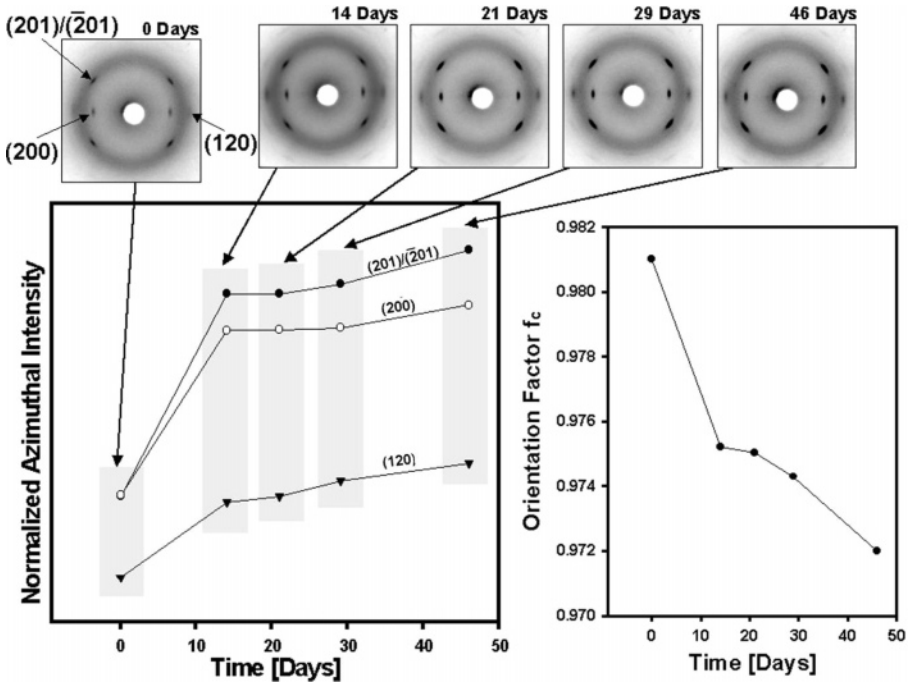

Figure 11. Crystallinity development of natural rubber stretched to 6× at 0, 14, 21, 29, and 46 days after stretching.

observed under pressure: i.e., increase the melting point through the Clapyron−Clausius equation and thereby bring the material to a supercooled state. By elevating the pressure, Edwards and Philips were able to grow lamellar kebab crystals on the shish crystals of prestrained *cis*-polyisoperene at room temperature.[3]

One possible contributor to the nucleation of the new crystallites on the shish crystals, though not verified in this study, could be the presence of nonrubber constituents, especially mixed fatty acids. It was recently proposed that the fundamental structure of natural rubber consists of an ω-terminal that forms

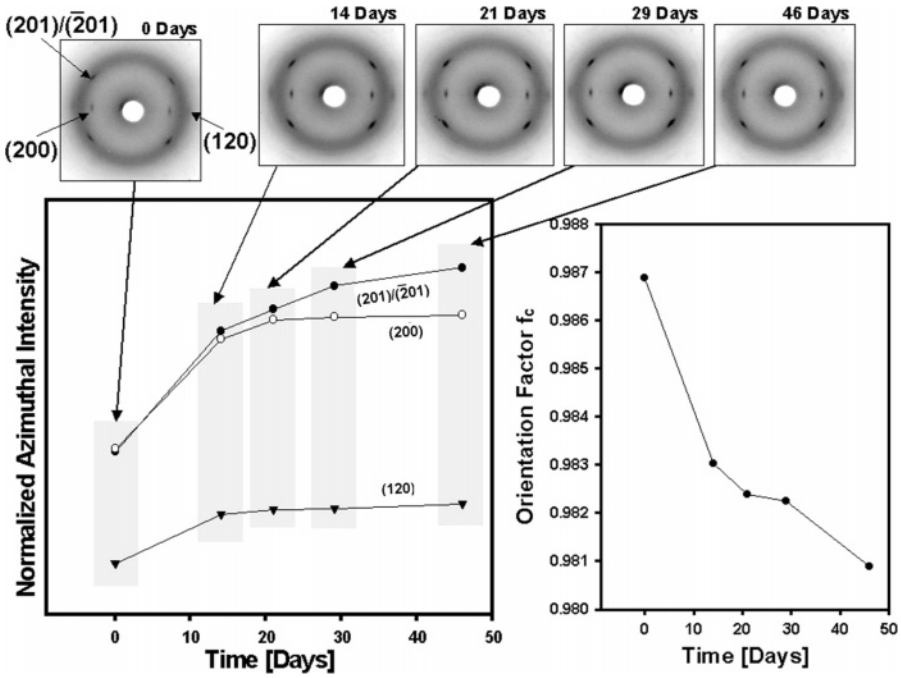

Figure 12. Crystallinity development of natural rubber stretched to 6× and then retracted to 5.5× at 0, 14, 21, 29, and 46 days after stretching.

branch points through hydrogen bonding between proteins, two *trans*-1,4 isoprene units, about 1000−5000 *cis*-1,4 isoprene units, and an α-terminal linking up with two or three fatty acids per rubber chain.[33] It was shown that the crystallization behavior of unstretched rubber was significantly promoted by the nucleating effect of the saturated fatty acids and plasticizing effect of the unsaturated ones[9,10] The presence of these nonrubber compounds could change the driving force for crystallization through both enthalpic and entropic reasons. Optical pictures in Figures 8−10 show that the crystallites are lined up along the direction of stretching. This strongly suggests that the crystallites nucleate on the shish crystals. If we were to attribute contribution to the secondary nucleation by the presence of fatty acids, we need to assume that all the fatty acids are linked to the natural rubber chains as phospholipids and hence are part of the shish crystals. Although the amount of linked fatty acids could be significant in a rubber chain, there should be reasonable population of the unlinked fatty acids. However, we do not observe independent growth of spherulites from the unlinked fatty acids in the stretched rubber. This clearly indicates that the long-term secondary crystallization nucleates on the shish structures. Further evidence will be given in the following sections.

The optical micrographs of the samples stretched to 6× and then retracted to 5.5× and 4× are observed in Figures 9 and 10, respectively. The observations for the sample stretched to 6×, and then retracted to 5.5× (Figure 9) are similar to that stretched to 6× only. However, the bright bands along the stretching direction are broader. The sample originally stretched to 6× and retracted to 4× (Figure 10) does not show any sign of crystallinity immediately after stretching as the X-ray pattern demonstrates a continuous amorphous halo. At the end of 47 days of storage period, the reflections of the crystalline planes (200) and (201)/(−201) are recognizable (see image enhanced portion in the WAXS pattern), indicating the formation of highly oriented crystalline domains. In addition, the optical micrographs

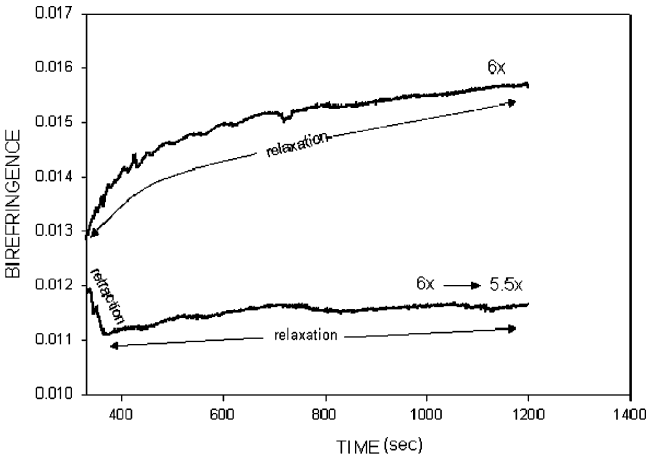

Figure 13. Comparison of the initial stages of the temporal development of birefringence during relaxation for samples stretched to 6× and samples stretched to 6× and retracted to 5.5×.

reveal the formation of crystals growing in the transverse direction, however, at a much lower density than the highly stretched samples.

3.2. X-ray Studies on the Development of Crystal Structure over Long Periods of Storage Time and the Effect of Partial Retraction. The crystallinity development with time was monitored using WAXS technique. X-ray patterns of natural rubber samples held in the strained state were taken at 0, 14, 21, 29, and 47 days after the stretching. Figures 11 and 12 shows the crystallinity development for a sample stretched to 6× and 6× followed by retraction to 5.5×, respectively.

The X-ray patterns show an increase in the crystalline peak intensities with time. Quantification of the area under the azimuthal scans of the (200), (120), and (201)/(−201) planes indicates a continuous increase with time; however, a larger step is found within the first 14 days after stretching. The azimuthal intensity for the (200) and (201)/(−201) crystallographic planes begins to level

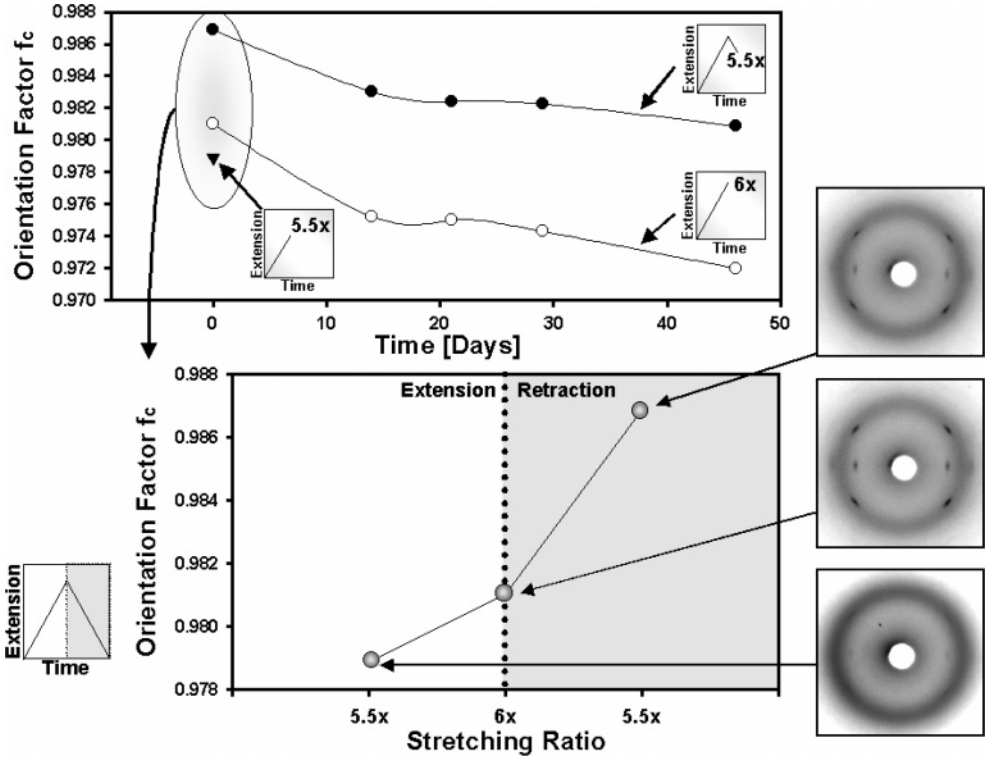

Figure 14. Orientation factors (f_c) of natural rubber stretched to 5.5×, 6×, and 6× and then retracted to 5.5× at 0, 14, 21, 29, and 46 days after stretching.

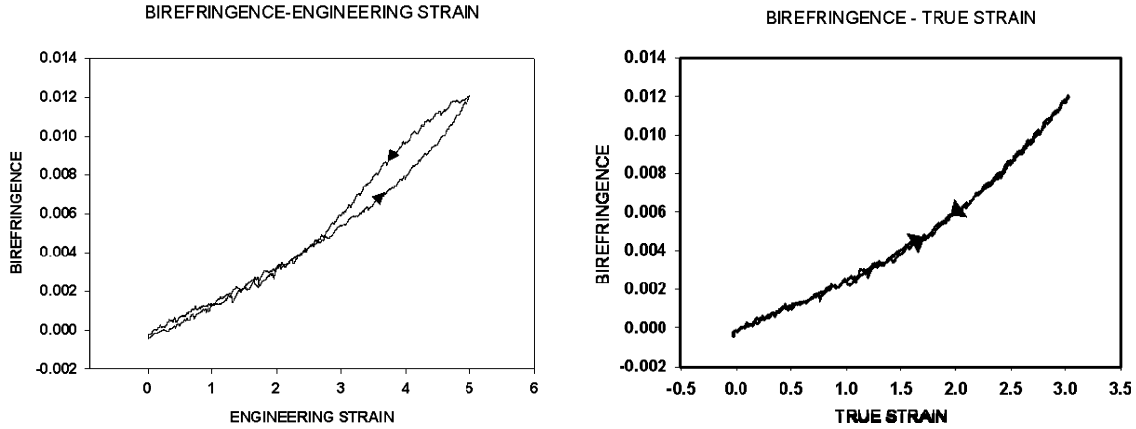

Figure 15. Birefringence vs engineering strain (left) and birefringence vs true strain (right) behavior during stretching to 6× and immediate full retraction.

off after 14 days indicating that most of the crystallization takes place during the first 14 days after the stretching.

The orientation factor f_c was calculated for each X-ray pattern. All of the values are very close to the ideal value of 1 indicating nearly perfect orientation of the crystalline structures along the stretching direction. However, a noticeable decrease of the orientation factor is observed within the first 14 days after stretching. This indicates that the crystallites forming during the constrained state are not as perfectly aligned as the ones formed during the stretching. The orientation factor continues to decrease at longer periods of time but at much lower rates. This decrease is inversely proportional to the crystallinity monitored by the peak intensity area of the azimuthal scans.

For the sample stretched to 6× and then retracted to 5.5× (Figure 12), an increase in crystallinity is observed during the first 14 days of constrained state, however in lower proportions compared to the unretracted counterpart. The ratio of the area under the azimuthal intensity (samples constrained for 14 days/freshly stretched) is larger for samples stretched to 6× (ratio: 2.3) than the samples stretched to 6× and then retracted to 5.5 (ratio: 1.6). This indicates that a higher rate of crystallinity developed in time for samples kept constrained at higher stretching ratios. This is evidenced in Figure 13 where the initial stages of the temporal development of birefringence for a sample stretched to 6× and a sample stretched to 6× and retracted to 5.5× are shown. Comparison of the relaxation periods shows that the birefringence increase during holding is faster for 6× than the sample stretched 6× and retracted to 5.5×.

The orientation factors are larger for the sample stretched to 6× and retracted to 5.5× than for the rubber stretched to 6× as shown in Figure 14. An additional orientation factor for a sample stretched to

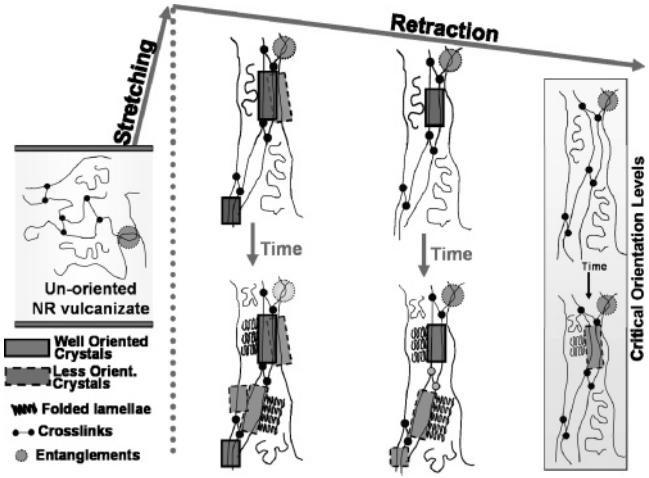

Figure 16. Model depicting the development of crystallites with time and effect of retraction on the structure.

5.5× is included for comparison purposes. The sample stretched to 5.5× shows lower degree of orientation. This is in accord with the lower values of birefringence recorded during the stretching of the sample (Figure 5) as compared to stretched and retracted to the same stretch ratio. Further stretching (6×) increases the molecular orientation along the stretching direction, as expected. However, the sample stretched to 6× and retracted to 5.5× shows even higher orientation values (yet lower crystallinity levels). This is attributed to the melting of the more imperfect crystals during retraction.

The stretching of rubber to high extensions leads to the formation of crystals with narrow orientation distribution. This orientation distribution includes highly oriented crystals that require larger energy to form and hence are thermodynamically more stable. The retraction to 5.5× is low enough to melt the less stable crystals (those exhibiting lower preferred orientation with respect to the stretching direction) but high enough for the more stable crystals to remain oriented in the stretching direction. As a result, higher crystalline orientation levels are achieved if a small relaxation is permitted. Figure 15 shows birefringence vs true strain during stretching to a stretch ratio of 6× followed by immediate retraction to the initial length of the film. Birefringence increases with stretching and follows completely the same route during retraction. This indicates that natural rubber crystals formed during stretching to 6× starts melting immediately with retraction. If the crystals were to resist melting during retraction, birefringence would exhibit a delay in its decrease during the initial stages of retraction. Recently it was reported that crystals did not melt immediately during retraction and were stable in the initial stages of retraction.[37] However, this is artificially introduced by representing mechanical data with engineering measure. With our real time measurement system, we can present both engineering and strain measures of the same data. This is shown in Figure 15. As observed, the engineering measure is not able to capture the true strain levels taking place at the same location, and therefore an artificial delay is seen during the retraction

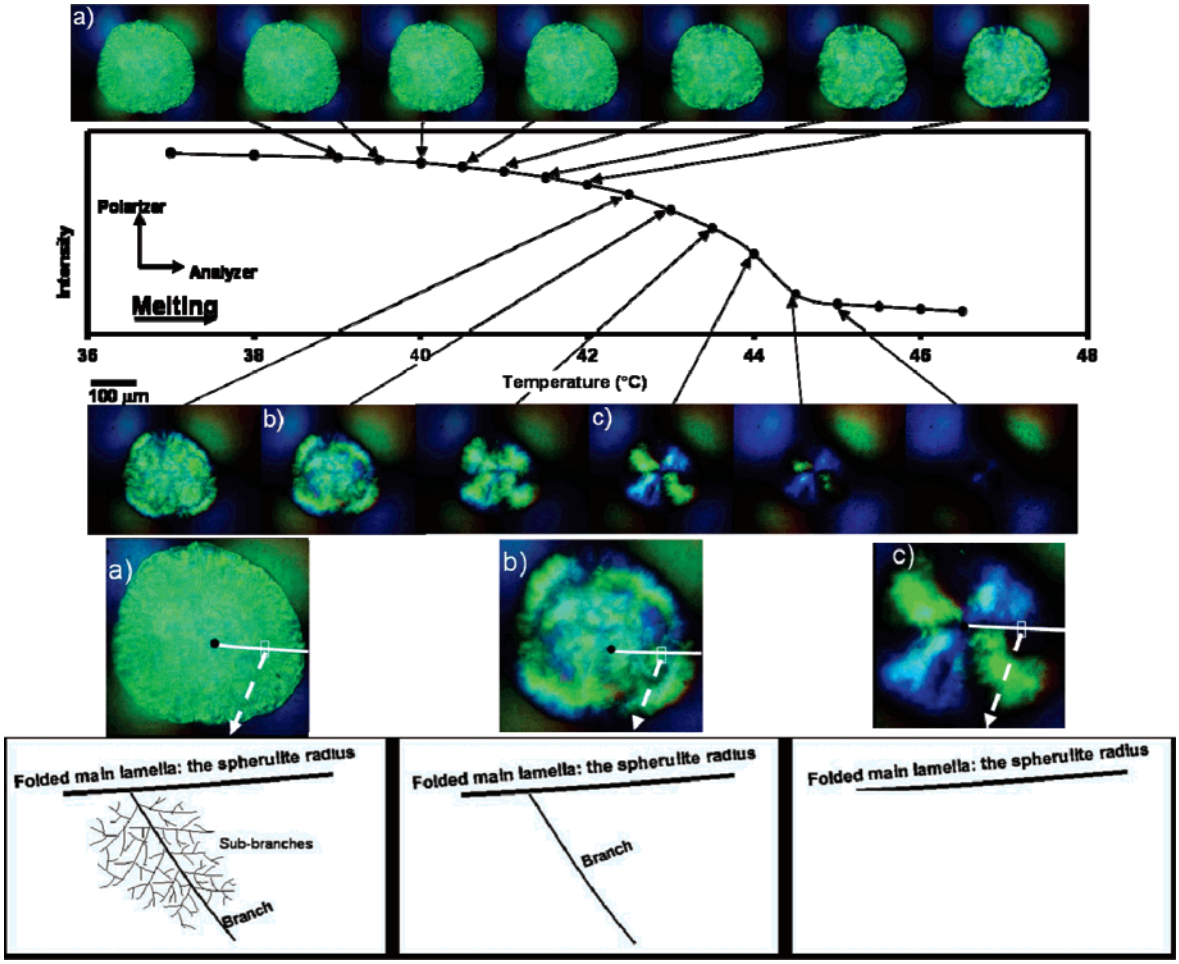

Figure 17. Melting behavior of unstretched natural rubber crystals monitored with optical measurements.

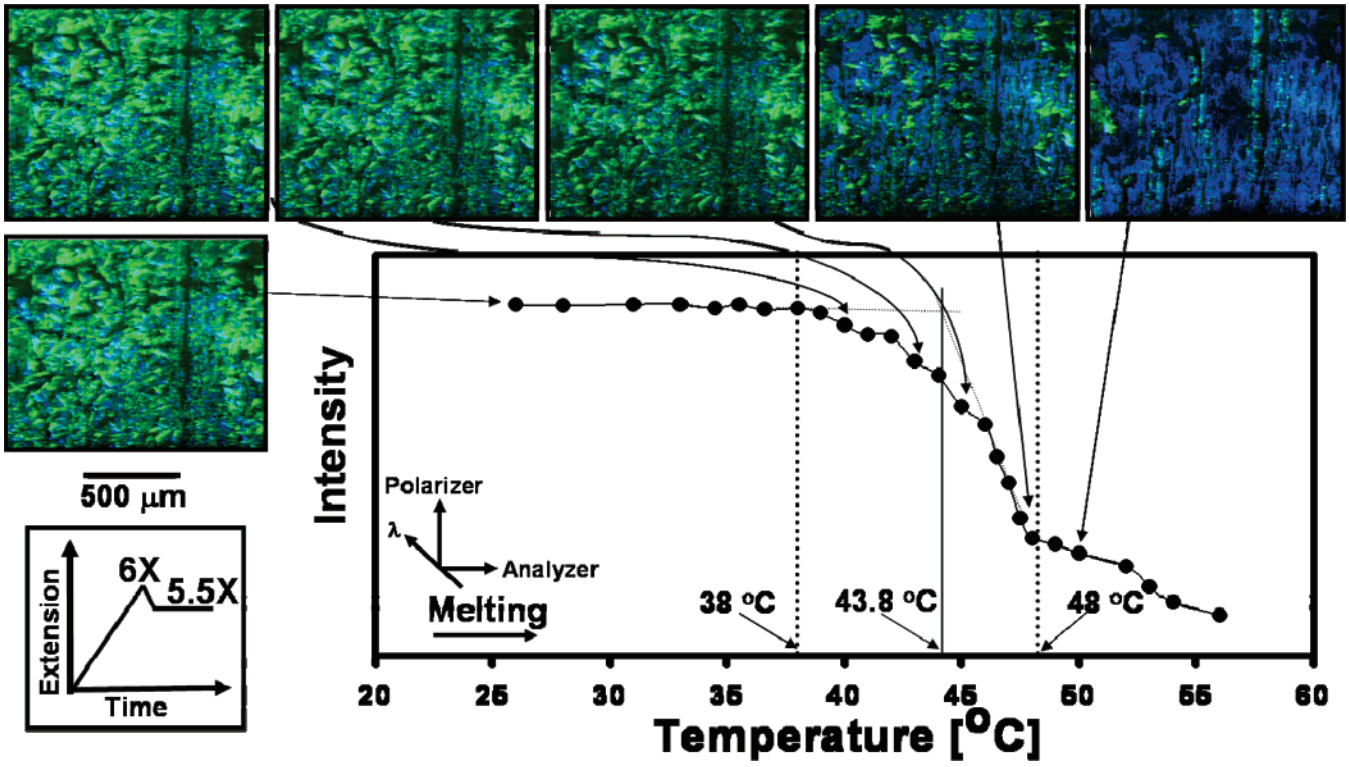

Figure 18. Melting behavior of stretched natural rubber crystals monitored with optical measurements (sample: 6× → 5.5× and kept for 10 months).

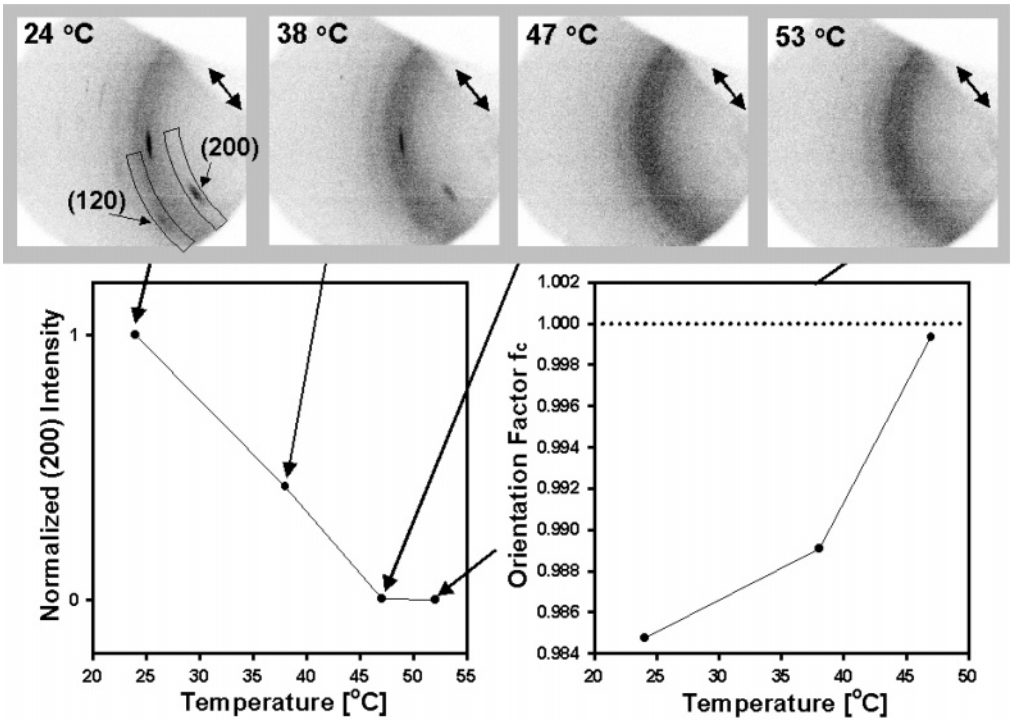

Figure 19. Melting behaviors of natural rubber crystals monitored with WAXS measurements. Orientation factors at different temperatures (sample: 6× and kept for 10 months).

cycle. However, when the data are plotted with the true strain measures, this delay is not observed. Therefore, we do not believe any delay in melting occurs during retraction.

A model is presented in Figure 16 illustrating the retraction-induced melting mechanism of the crystallites with differing degrees of orientation with respect to the stretching direction and subsequent lateral overgrowths over long periods of time. The model shows that uniaxial stretching of natural rubber results in the immediate formation of orientation-induced crystals with differing degrees of orientation. Immediate retraction after stretching results in the melting of those with less perfect orientation depicted with dashed line boundary in this figure. Further retraction results in complete melting of the crystals, including the well oriented ones. The

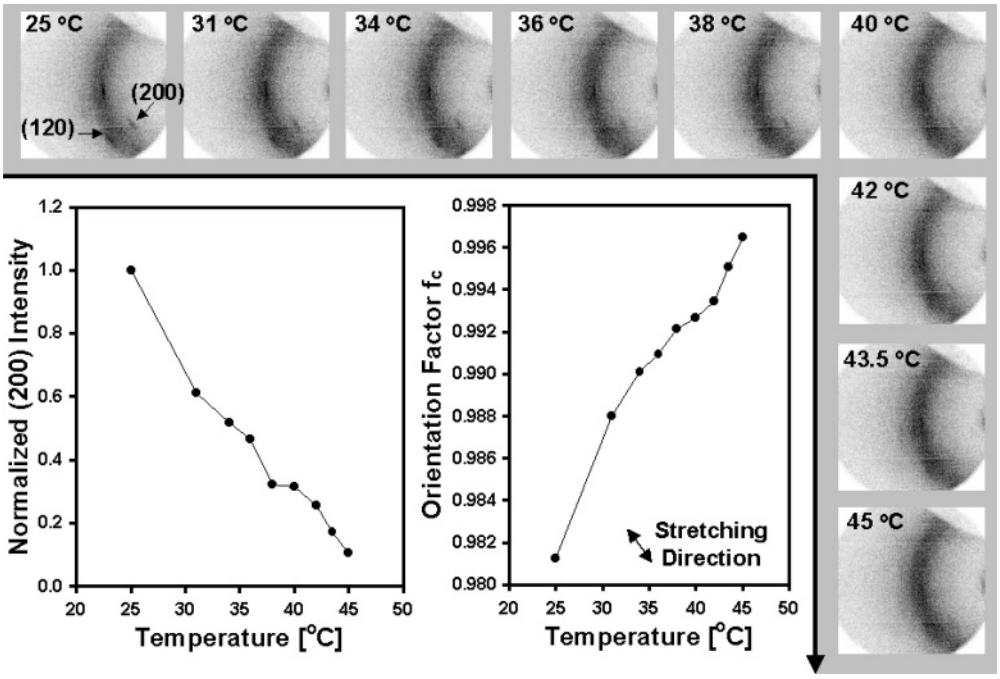

Figure 20. Melting behavior of stretched (6×) natural rubber crystals monitored with WAXS measurements. Orientation factors at different temperatures.

model also shows that, given enough time, the lateral crystal overgrowths develop on the oriented crystals either remaining from the stretching stage or developed during the early stages of the long-term holding following retraction.

3.3. Crystalline Melting Behavior. Natural rubber stored for long periods of time develops large crystalline structures randomly distributed in the rubber matrix. Figure 17 shows the melting behavior of an unstretched natural rubber vulcanizate sample stored for 10 months. This sample exhibits clear spherulitic structure. Melting takes place in a range of temperatures of about 6 °C, from 39 to 45 °C. At 44 °C, there is an appearance of the Maltese cross pattern under cross polars that is not observed at lower temperatures when the crystal is larger. This indicates that at the interior the lamellae originally grow radially from a preexisting nuclei forming classical spherulitic structure. At longer crystallization times, the secondary crystallization alters this spherulitic optical symmetry to eliminate the Maltese cross. It is possible that at long duration the volume filling crystallization involves substantial sub-branching of lamellae from the main branches. This would certainly suppress the macroscopic Maltese cross appearance by promoting local optical isotropy. During heating, the small sub-branches that possess lower melting peaks disappear first, leaving the original radial lamellae that in turn exhibit a Maltese cross appearance under crossed polars before their disappearance above the melting regime. The melting temperature of these spherulites is much higher than the reported equilibrium melting temperatures. This is not surprising since these crystals were grown very slowly over long periods of time at room temperature. Similar high-temperature crystallites were found in stark natural rubber stored for long periods of time.[38] Crystallites formed at low (−25 °C) and high temperature (room temperature) are distinguished by the degree of their development and perfection but pertain to the same crystallographic form.[39] Although long-term slow crystallization at room temperature is necessary, it is not sufficient to grow high temperature crystallites in natural rubber. The previous history of the rubber, specifically exposing the rubber to compressional stress by pressing, calendaring, and even masticating, was found to be influential.

The melting behavior of stretched natural rubber samples was also monitored with depolarized light intensity analysis. The results are shown in Figure 18 for a natural rubber stretched to 6× and then retracted to 5.5× and kept in the strained state for 10 months. The lateral overgrowth crystals disappear in the 38−48 °C temperature range. Above 48 °C, the rate of melting slows down, and we observe crystallites that are organized along vertical lines—presumably nearest to the shish crystals—that persist to temperatures as high as 57 °C.

However, this experimentation does not provide information about the melting mechanism of the extended chain crystals along the stretching direction. That is the reason we resorted to the melting behavior of stretched rubber using the WAXS technique. In this series of experiments the samples remain in the stretched state in the sandwich-clamps (Figure 2), they were captured in following their deformation. In this experiment, the heating is provided by a radiant heat source directly on the sample while the temperature of the spot where the X-ray beam intersects the sample is measured continuously by an infrared pyrometer. These experiments were perfomed in a step-heating manner. Figure 19 shows the melting behavior of a rubber sample stretched to 6× and kept in the strained state for 10 months. The melting transition is monitored by the examination of the (200) planes' integrated azimuthal intensity corrected for amorphous background. The integrated intensity of the (200) planes continuously decreases with temperature indicating the melting transition of the highly oriented crystals. The presence of crystalline structures at 47 °C shows that the melting temperature shifts to higher values as compared to the reported equilibrium melting temperature of unstretched

fresh *cis*-polyisoprene[14,16,17] This is due to higher thermal stability of the oriented structures. The crystalline chain orientation factor increases with increasing temperature. The original strain-induced crystals exhibit a very narrow orientation distribution with respect to the stretching direction. The more unstable crystals (∼less perfect and/or smaller) are the ones that first melt as the temperature is increased. These are the crystals possessing lower orientation and oriented in the direction away from the stretching direction. The crystals possessing higher orientation remain intact well into higher temperatures without losing their orientation and are the last ones to melt. It should be noted that the optical data shown in Figure 18 indicates that structural anisotropies persist up to 57 °C, about 10 °C above the temperature where the crystalline peaks disappear from WAXS patterns. We attribute this discrepancy to the insensitivity of the WAXS technique at these very low crystallinity levels.

Figure 20 shows the same melting transition experiment for a rubber sample stretched to 6× and measured immediately. Similar behavior is seen in both types of stretched rubber. i.e., fresh and kept for 10 months.

4. Conclusions

Optical microscopy measurements on stretched natural rubber samples reveal the lateral growth of crystalline structures. The mechanism of formation of long-term crystals is attributed to the preferential orientation developed during stretching in the amorphous regions surrounding the shish structures that decrease with distance from the center of each shish. The spatial density of these crystals decrease with time (distance from center of each shish) leading to clear observation of individual platelike crystallites away from the shishes as the supercooling effect gradually diminish.

WAXS measurements on stretched natural rubber samples indicate substantial crystallinity development with time at room temperature. Most of the post-stretching crystallinity takes place within the first 14 days after the stretching. The newly formed crystals exhibit lower values of crystalline orientation along the stretching direction. The natural rubber stretched to 6× and retracted to 5.5× shows higher orientation levels in crystalline regions with lower crystallinity than the sample stretched to 6×, indicating retraction-induced melting of the crystal population with lower preferential orientation along the stretching direction.

The temperature-induced melting mechanism of highly oriented crystalline structures was also investigated. WAXS indicates that the crystallinity continuously decreases with temperature up to about 48 °C. Depolarized light intensity measurements shows that optically anisotropic entities persist up to 57 °C. Crystals with high orientation remain crystallized without losing their orientation and are the last ones to melt.

References and Notes

(1) Andrews, E. H. *Proc. R. Soc. Ser A* **1962**, *270*, 232−241.
(2) Philips, P. J.; Edwards, B. C. *J. Polym. Sci., Polym. Phys. Ed*. **1975**, *13*, 1819−1829.
(3) Philips, P. J.; Edwards, B. C. *J. Polym. Sci., Polym. Phys. Ed.* **1975**, *13*, 2117−2127.
(4) Gent, A. N. *Trans Faraday Soc.* **1954**, *50*, 521.
(5) Andrews, E. H. *Proc. R. Soc. London, Ser. A* **1964**, *277*, 562−570.
(6) Manzur; McIntyre, D. *J. Macromol. Sci., Phys. B* **1988**, *27* (1), 79−98.
(7) Bateman, L. *The Chemistry and Physics of Rubber-like Substances*; John Wiley & Sons: New York, 1963.
(8) Trabelski, S.; Albouy, P. A.; Rault, J. *Macromolecules* **2003**, *36*, 7624−7639.
(9) Kawahara, S.; Kakubo, T.; Sakdapipanich, J. T.; Isono, Y.; Tanaka, Y. *Polymer* **2000**, *41*, 7483−7488.
(10) Kawahara, S.; Takano, K.; Yunyongwattanakorn, J.; Isono, Y.; Hikosaka, M.; Sakdapipanich, J. T.; Tanaka, Y. *Polym. J.*, **2004**, *36*, (5), 361−367.
(11) Tarachiwin, L.; Sakdapipanich, J. T.; Tanaka, Y. *Rubber Chem. Technol.* **2003**, *76*, 1177−1184.
(12) Yunyongwattanakorn, J.; Tanaka, Y.; Kawahara, S.; Klinklai, W.; Sakdapipanich, J. *Rubber Chem. Technol.* **2003**, *76*, 1228−1240.
(13) Kawara, S.; Kakubo, T.; Suzuki, M.; Tanaka, Y *Rubber Chem. Technol.* **1999**, *72* (1), 174−180.
(14) Dalal, E. N.; Taylor, K. D.; Phillips, P. J. *Polymer* **1983**, *24*, 1623−1630.
(15) Dalal, E. N.; Taylor, K. D.; Phillips, P. J. *Macromolecules* **1983**, 16, 1754−1760.
(16) Bekkedahl, N. *Rubb. Chem. Technol*. **1967**, *40*(3), xxv−xlvii.
(17) Maynard, J. T.; Mochel, W. E. *J. Polym. Sci.* **1954**, *13*, 235.
(18) Scott, R. G. *Symp. Microsc. Am. Soc. Test. Mater. Spec. Technol. Publ*. **1959**, 257.
(19) Shimizu, T.; Tosaka, M.; Tsuji, M.; Kohjiya, S. *Rubber Chem. Technol.* **2000**, *73*, 926−936.
(20) Edwards, B. C. *J. Polym. Sci.* **1975**, Vol. 13, 1387−1405.
(21) Edwards, B. C.; Phillips, P. J.; Sorenson, D. *J. Polym. Sci., Phys. Ed*. **1980**, *18*, 1737−1745.
(22) Phillips, P. J.; Edwards, B. C. *J. Polym. Sci., Phys. Ed.* **1976**, *14*, 377−389.
(23) Phillips, P. J.; Edwards, B. C. *J. Polym. Sci., Phys. Ed.* **1980**, *18*, 1737−1745.
(24) Tosaka, M.; Murakami, S.; Poompradub, S.; Kohjiya, S.; Toki, S.; Sics, I.; Hsiao, B. S. *Macromolecules* **2004**, *37*, 3299−3309.
(25) Toki, S.; Hsiao, B. S. *Macromolecules* **2003**, *36*, 5915−5917.
(26) Koike, Y.; Cakmak, M. *Polymer* **2003**, *44*, 4249−4260.
(27) Beekmans, F.; Posthuma de Boer, A. *Macromolecules* **1996**, *29*, 8726−33.
(28) Nyburg, S. C. *British J. Appl. Phys.*. **1954**, *5*, 321−324.
(29) Bunn, W. *Proc. R. Soc. (London)* **1942**, *A180*, 40−66.
(30) Magill, J. H. *Rubber Chem. Technol.* **1995**, *68*, 507−539.
(31) Wilchinsky, Z. W. *Polymer* **1964**, *5*, 271−281.
(32) Mitchell, G. R. *Polymer* **1984**, *25*, 1562.
(33) Tanaka, Y.; Kawara, S.; Tangpakdee, J. *Kautsch. Gummi Kunst* **1977**, *50*, 6.
(34) Suzuki, A.; Oikawa, H.; Murakami, K. *Polymer* **1985**, *26*, 247−252.
(35) Flory, P. J. *J. Chem. Phys.* **1947**, *15*, 397.
(36) Mulligan, J.; Cakmak, M. *Macromolecules* **2005**, *38*, 2333−2344.
(37) Toki, S.; Sics, I.; Ran, S.; Liu, L.; Hsiao, B. S. *Polymer* **2003**, *44*, 6003−6011.
(38) Roberts, D. E.; L. Mandelkern. *J. Res. Nat. Bur. Stand.* **1955**, *54* (3), 167−176.
(39) Teitel'baum, B. Ya.; Anoshina, N. P. *Vysokomol. Soedin.* **1965**, *7*, 2112−2116.

MA050413Q